Unconventional superconducting phases in multilayer films with layer-dependent Rashba spin-orbit interactions

Ryuichi Masutomi,[*] and Tohru Okamoto
Department of Physics, University of Tokyo, Tokyo 113-0033, Japan

Youichi Yanase
Department of Physics, Kyoto University, Kyoto 606-8502, Japan

We present resistivity measurements of bilayer and trilayer films with layer-dependent Rashba spin-orbit interactions. A sharp upturn is observed in the temperature dependence of the parallel upper critical field. We show that it corresponds to a transition from a complex-stripe phase to a helical phase. Moreover, we propose the phase diagram of a multilayer system, which is obtained from experimental observations with the support of numerical calculations. These results pave the way for the clarification of non-trivial superconducting states in multilayer systems composed of two-dimensional Rashba superconductors.

The Rashba spin-orbit interaction (SOI) is a relativistic effect caused by uniaxial space-inversion-symmetry breaking [1]. It has been known to play an important role not only in the development of next-generation spintronic devices, but also in the emergence of superconducting states, which is beyond the conventional Bardeen–Cooper–Schrieffer (BCS) framework [2–5]. Recently, Yanase *et al.* presented several theoretical studies on superconducting states in multilayer systems composed of two-dimensional (2D) superconductors with layer-dependent Rashba SOIs [6–9]. In these systems, unconventional superconducting phases, e.g., a complex-stripe (CS) phase characterized by both magnitude and phase modulations of the order parameter and a helical phase characterized by phase modulation of the order parameter, are expected to emerge in the presence of a magnetic field applied parallel to the 2D plane. However, no direct evidence supporting the existence of the CS phase and the helical phase with a spatially oscillating order parameter has been reported.

Figure 1 shows superconducting phases predicted for multiple monolayer systems in a parallel magnetic field $H^\parallel$ [7]. In the bilayer system [Fig. 1(a)], the sign of α_m changes for each layer due to an opposite potential gradient along the normal direction of the 2D plane (z direction), where α_m is the Rashba spin-orbit coupling of the mth layer ($m = 1, 2, \ldots$). When adjacent-layer hopping $t_\perp$ is zero or very small, the helical state with a phase-oscillating order parameter [10] is stable for each layer even in low magnetic fields. For $t_\perp \neq 0$, the inter-layer Josephson effect favors the conventional BCS state with a uniform order parameter in low magnetic fields. In high magnetic fields, on the other hand, two CS phases of different origins and with a finite $\boldsymbol{q}$ are expected: one is caused by the

Rashba SOI [6], and the other is induced by $H^\parallel$ penetrating between the layers [7]. While the CS phases are similar to the helical phase for $t_\perp = 0$, the interlayer Josephson effect leads to magnitude modulation of the order parameter. Which CS phase is chosen is determined by the competition between the Rashba SOI (paramagnetic effect) and the orbital effect [7]. In the trilayer system [Fig. 1(b)], the local inversion symmetry is not broken in the second (intermediate) layer. In the CS phase, the second layer is in the Larkin–Ovchinnikov (LO) state [11], while the first and third layers are in the CS state.

Recently, advances in thin-film growth technology have led to the fabrication of one-atomic-layer-thick 2D superconductors [12–14]. Since these superconducting monolayer films are grown on a semiconductor surface, the Rashba-type SOI is expected to be caused by the lack of space inversion symmetry in the z direction. Actually, in the monolayer Tl-Pb film on Si(111) with a large Rashba spin splitting of $\sim$250 meV at the Fermi level ε_F (as measured by angle-resolved photoelectron spectroscopy), superconductivity has been observed by using the micro-four-point-probe method [15] and scanning tunneling spectroscopy [16]. Furthermore, two of the current authors found that the superconducting transition temperature T_c decreases by only a few percent in parallel magnetic fields exceeding by several times the Pauli paramagnetic limit [17,18] in monolayer Pb films grown on cleaved GaAs(110) surfaces [19,20]. The weak dependence of T_c on $H^\parallel$ was quantitatively explained in terms of an inhomogeneous superconducting state predicted for 2D metals with a large Rashba spin splitting [3,4]. In the present study, we exploit monolayer Pb films with a strong Rashba SOI to search for nontrivial superconducting states in multilayer systems with layer-dependent Rashba SOIs. From the measurements on the temperature dependence of the parallel upper critical field $H_{c2}^\parallel$ and the numerical calculations based on the Bogoliubov–de Gennes (BdG) equations, we suggest that $H^\parallel$ penetrating
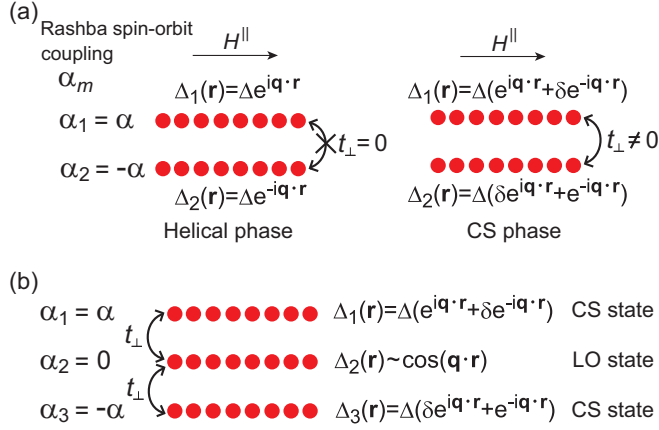
*masutomi@phys.s.u-tokyo.ac.jp

184502-1

FIG. 1. Superconducting phases in multiple monolayer systems. (a) Theoretical model for a bilayer system in a parallel magnetic field $H^{\parallel}$. The row of red circles denotes the 2D superconductor with α_m, where α_m is the Rashba spin-orbit coupling of the mth layer. When each layer is decoupled from the other layer ($t_\perp = 0$), the superconducting order parameter of the upper (lower) layer is given by $\Delta_1(\mathbf{r}) = \Delta e^{i\mathbf{q} \cdot \mathbf{r}}$ [$\Delta_2(\mathbf{r}) = \Delta e^{-i\mathbf{q} \cdot \mathbf{r}}$] as the helical phase with a finite center-of-mass momentum $\mathbf{q}$ ($-\mathbf{q}$). In contrast, when each layer is coupled to the other layer ($t_\perp \neq 0$), using interlayer Josephson coupling δ, Δ_1 (Δ_2) is given by $\Delta_1(\mathbf{r}) = \Delta(e^{i\mathbf{q} \cdot \mathbf{r}} + \delta e^{-i\mathbf{q} \cdot \mathbf{r}}) \simeq \Delta e^{i\mathbf{q} \cdot \mathbf{r}}[1 + \delta^2 + 2\delta \cos(2\mathbf{q} \cdot \mathbf{r})]^{1/2}$ $\{\Delta_2(\mathbf{r}) = \Delta(\delta e^{i\mathbf{q} \cdot \mathbf{r}} + e^{-i\mathbf{q} \cdot \mathbf{r}}) \simeq \Delta e^{-i\mathbf{q} \cdot \mathbf{r}}[1 + \delta^2 + 2\delta \cos(2\mathbf{q} \cdot \mathbf{r})]^{1/2}\}$ as the complex-stripe (CS phase, which is characterized by both phase and magnitude modulations. (b) Theoretical model for the CS phase of a trilayer system in $H^{\parallel}$. In the second (intermediate) layer, local space inversion symmetry is preserved; therefore, Δ_2 for the second layer is given by $\Delta_2(\mathbf{r}) \sim e^{i\mathbf{q} \cdot \mathbf{r}} + e^{-i\mathbf{q} \cdot \mathbf{r}} \sim \cos(\mathbf{q} \cdot \mathbf{r})$ as the Larkin-Ovchinnikov (LO) state.

between the layers induces a transition from the CS phase to the helical phase.

To investigate superconducting states in multiple monolayer systems, we fabricated bilayer and trilayer films on a cleaved GaAs surface, as depicted in the insets of Figs. 2(a)
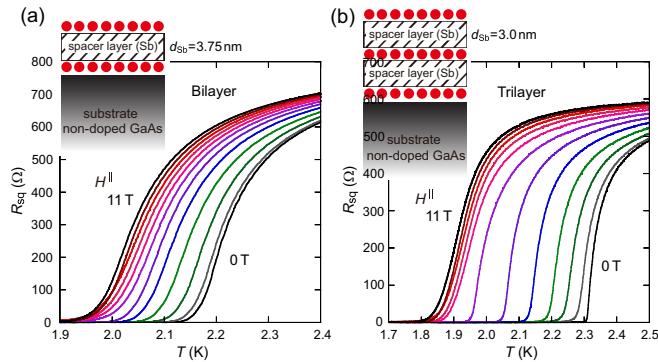
and 2(b). Following the cleavage of an undoped insulating GaAs single-crystal in an ultrahigh vacuum chamber, Pb and Sb were thermally deposited onto the cleaved (110) surface. Here, the substrate was cooled down to liquid helium temperatures to prevent the thermal diffusion of atoms, which may cause grain formation and intermixing of Pb and Sb atoms. Note that the Pb films are not expected to be completely epitaxially smooth as illustrated in the insets of Fig. 1. The amount of Pb or Sb deposited was measured by using a quartz crystal microbalance and determined with an accuracy of about 5%. Current and voltage electrodes were prepared in advance by depositing gold films onto noncleaved surfaces [19–21]. The four-probe resistance of bilayer and trilayer films grown on cleaved GaAs(110) surfaces (4×0.35 mm^2) was measured *in situ* by using a standard lock-in technique. The magnetic-field direction with respect to the surface normal was precisely controlled by using a rotary stage on which the sample was mounted, together with a Hall sensor, a RuO$_2$ resistance thermometer and a heater (see Sec. I of the Supplemental Material [22]). The sample stage was cooled down to 0.5 K via a silver foil linked to a pumped ^{3}He refrigerator. All the data were taken when the temperature of the sample stage was kept constant so as to ensure thermal equilibrium between sample and thermometer. The magnetoresistance effect of the RuO$_2$ resistance thermometer was systematically calibrated against the vapor pressure of ^{3}He or ^{4}He for various temperatures [23]. After the correction, T_c was determined with a relative accuracy better than 0.2%.

In this study, the coupling strength between Pb monolayer films was controlled by changing the thickness of an Sb spacer layer. We verified that the deposition of the Sb spacer layer does not overly affect the basic superconducting properties of the monolayer Pb film (8.9 nm^{-2}), *e.g.*, the zero-field superconducting transition temperature T_{c0} and the normal-state sheet resistance R_N (see Sec. II of the Supplemental Material [22]). Moreover, T_{c0} for the bilayer and trilayer films is nearly identical to or slightly greater than that for a pristine monolayer Pb film, suggesting that the multiple-monolayer Pb films with Sb spacer layers work well as weakly coupled systems. We made magnetotransport measurements on the bilayer and trilayer films for different Sb thickness d_{Sb} from 3.0 to 3.75 nm. Figure 2 shows the sheet resistance R_{sq} as a function of temperature for the bilayer film with $d_{Sb} = 3.75$ nm [Fig. 2(a)] and the trilayer film with $d_{Sb} = 3.0$ nm [Fig. 2(b)]. The broadening of the superconducting transition by fluctuations is similar to that for monolayer films [13,15,19], and does not depend significantly on $H^{\parallel}$ while T_c decreases with $H^{\parallel}$.

In Fig. 3, we plot $H_{c2}^{\parallel}$ and the perpendicular upper critical field $H_{c2}^{\perp}$ as a function of T/T_{c0} for bilayer and trilayer films with different d_{Sb}, where $H_{c2}^{\parallel}$, $H_{c2}^{\perp}$ and T_{c0} are determined from the midpoint of the resistive transition. While $H_{c2}^{\perp}$ exhibits a linear temperature dependence [24], $H_{c2}^{\parallel}$ shown in Figs. 3(a)–3(c) varies as the square root of $(1 - T/T_{c0})$. Since the value of $H_{c2}^{\parallel}/\sqrt{1 - T/T_{c0}}$ is 10–30 times smaller than that for the monolayer Pb film [19], the reduction of $H_{c2}^{\parallel}$ is mainly attributed to the formation of multilayer structures. It can be explained in the BCS framework. On the basis of the Ginzburg–Landau (GL) theory applied to interacting
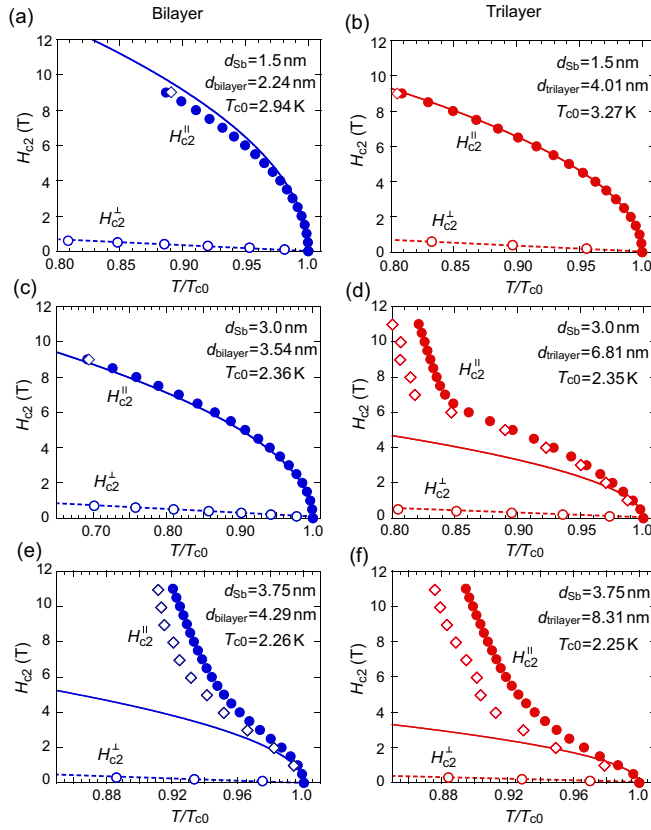

FIG. 2. Superconducting transition in multiple monolayer films. (a), (b) Sheet resistance R_{sq} as a function of temperature T for (a) bilayer film with $d_{Sb} = 3.75$ nm and (b) trilayer film with $d_{Sb} = 3.0$ nm in parallel magnetic fields $H^{\parallel}$, varying in 1 T steps from 0 to 11 T. The insets of panels (a) and (b) show the schematic drawing of the bilayer and trilayer films, respectively.

FIG. 3. Parallel and perpendicular upper critical magnetic fields of multiple monolayer films. (a)–(f) Temperature dependence of H_{c2} for the bilayer and trilayer films for different thickness d_{Sb} of an Sb spacer layer. The closed (open) circles denote the data of $H_{c2}^{\parallel}$ ($H_{c2}^{\perp}$), which are determined from the midpoint of the resistive transition. The dashed lines are linear fits to $H_{c2}^{\perp}$, from which $\xi_{GL}(0)$ is obtained. The solid blue (red) lines are obtained by substituting $\xi_{GL}(0)$ and $d_{bilayer} = d_{Sb} + 2d_{Pb}$ ($d_{trilayer} = 2d_{Sb} + 3d_{Pb}$) into Eq. (1) [Eq. (2)] for each bilayer (trilayer) film (see text). The open diamonds denote the data of $H_{c2}^{\parallel}$, which are determined from T_c at which zero resistance is observed.

superconducting layers, $H_{c2}^{\parallel}$ is given by

$$H_{c2}^{\parallel}(T) = \frac{2\Phi_0}{2\pi \xi_{GL}(0) d_{bilayer}} \sqrt{1 - T/T_{c0}} \quad \text{(bilayer)}, \quad (1)$$

and

$$H_{c2}^{\parallel}(T) = \frac{\sqrt{6}\Phi_0}{2\pi \xi_{GL}(0) d_{trilayer}} \sqrt{1 - T/T_{c0}} \quad \text{(trilayer)}, \quad (2)$$

for bilayer and trilayer, respectively. Here, Φ_0, $\xi_{GL}(0)$ and $d_{bilayer}$ ($d_{trilayer}$) denote the flux quantum, the in-plane GL coherence length at $T = 0$ K and the bilayer (trilayer) film thickness, respectively. The value of $\xi_{GL}(0)$ can be experimentally determined from

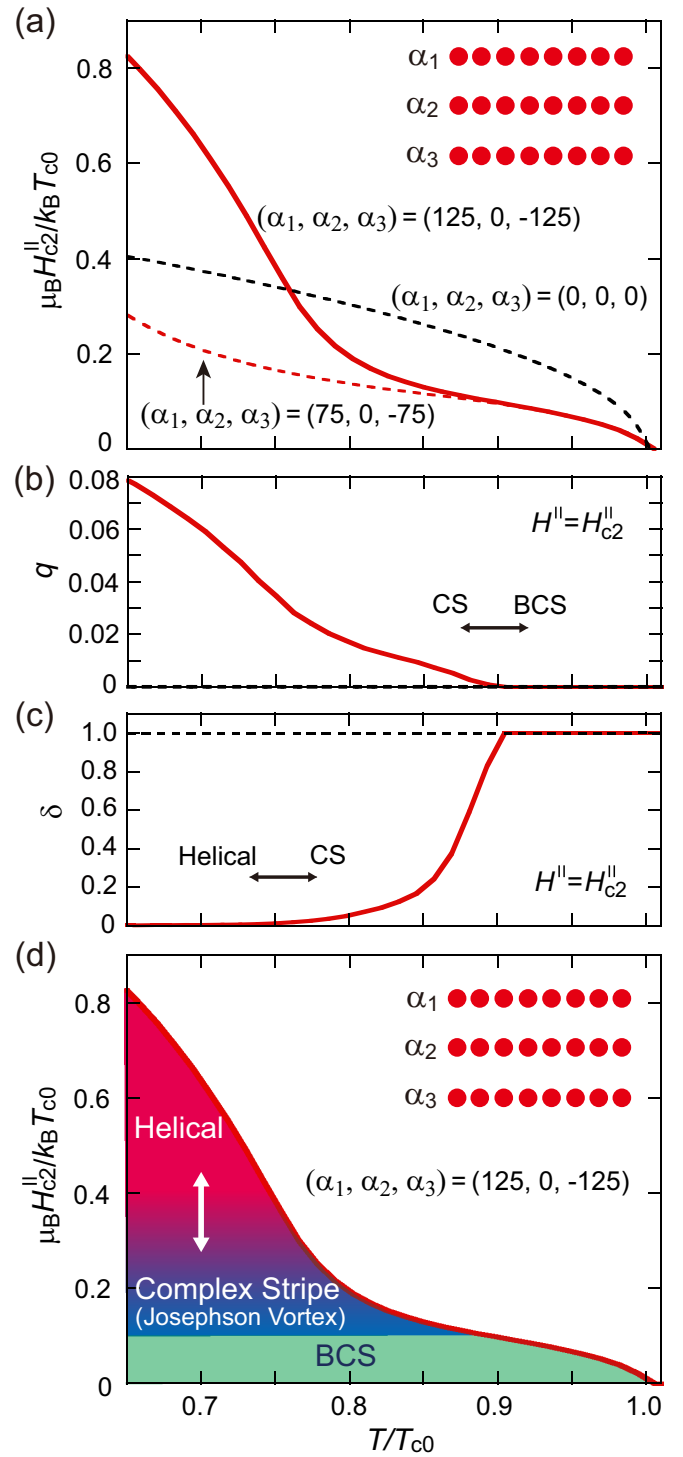$$H_{c2}^{\perp}(T) = \frac{\Phi_0}{2\pi \xi_{GL}(0)^2} (1 - T/T_{c0}). \quad (3)$$

FIG. 4. Theoretical calculation for superconducting states of trilayer systems. (a) Numerical calculations of $\mu_B H_{c2}^{\parallel}/k_B T_{c0}$ as a function of T/T_{c0} with different Rashba spin-orbit coupling $(\alpha_1, \alpha_2, \alpha_3) = (125, 0, -125)$ (solid red line), $(\alpha_1, \alpha_2, \alpha_3) = (75, 0, -75)$ (dashed red line) and $(\alpha_1, \alpha_2, \alpha_3) = (0, 0, 0)$ (dashed black line), where the unit of Rashba spin-orbit coupling α_m is in meV. (b),(c) Center-of-mass momentum q and the interlayer Josephson coupling δ as a function of T/T_{c0} at $H^{\parallel} = H_{c2}^{\parallel}$. (d) Phase diagram for the trilayer system with $(\alpha_1, \alpha_2, \alpha_3) = (125, 0, -125)$.

We find that $\xi_{\text{GL}}(0)$ has nearly the same values [$\xi_{\text{GL}}(0) = 10 \pm 1$ nm] for all the multilayer films. The temperature dependence of $H_{\text{c2}}^{\parallel}$ calculated by putting $\xi_{\text{GL}}(0)$ and the film thickness into Eq. (1) [Eq. (2)] is shown by solid blue (red) lines in Figs. 3(a)–3(f), and reasonably reproduces the experimental results shown in Figs. 3(a)–3(c). In contrast, in Figs. 3(d)–3(f), a sharp upturn is observed at high magnetic fields. Although the temperature dependence of $H_{\text{c2}}^{\parallel}$ in the low-magnetic-field region is also quantitatively explained by Eq. (1) or Eq. (2), the observed upturn of $H_{\text{c2}}^{\parallel}$ cannot be explained in the BCS framework.

The upturn of $H_{\text{c2}}^{\parallel}$ might be explained qualitatively using the model depicted in Fig. 1. In the numerical calculations with the BdG equations, we use a tight-binding model with in-plane hopping $t = 250$ meV leading to $\varepsilon_{\text{F}} \sim 500$ meV and $t_{\perp} = 25$ meV. The detailed method of numerical calculation is presented in Sec. III of the Supplemental Material [22]. Figure 4(a) shows the calculation of $\mu_{\text{B}} H_{\text{c2}}^{\parallel}$ normalized by $k_{\text{B}} T_{\text{c0}}$ for trilayer systems with $(\alpha_1, \alpha_2, \alpha_3) = (125, 0, -125)$, $(75, 0, -75)$ and $(0, 0, 0)$ in meV, where μ_{B} is the Bohr magneton and k_{B} is the Boltzmann constant. When the Rashba SOIs are zero [$(\alpha_1, \alpha_2, \alpha_3) = (0, 0, 0)$], the sharp upturn does not occur. In contrast, it appears for $(\alpha_1, \alpha_2, \alpha_3) = (125, 0, -125)$. The magnitude of the Rashba spin-orbit couplings ($|\alpha_{1(3)}| = 125$ meV) is comparable with the experimental values for similar systems [15,25]. Therefore, we consider that the layer-dependent Rashba SOIs play a key role in determining the temperature dependence of $H_{\text{c2}}^{\parallel}$ for the trilayer film.

Figure 4(d) presents the phase diagram for the trilayer system, which was obtained from the temperature dependence of q [Fig. 4(b)] and the interlayer Josephson coupling δ [Fig. 4(c)] at $H^{\parallel} = H_{\text{c2}}^{\parallel}$ for $(\alpha_1, \alpha_2, \alpha_3) = (125, 0, -125)$. In low-magnetic fields (i.e., $0.9 < T/T_{\text{c0}} < 1.0$ for $H^{\parallel} = H_{\text{c2}}^{\parallel}$), the BCS state with $q = 0$ (i.e., a uniform order parameter) is stable. In contrast, in high-magnetic fields ($T/T_{\text{c0}} < 0.9$ for $H^{\parallel} = H_{\text{c2}}^{\parallel}$), two types of superconducting states with nonzero q of Cooper pairs are stabilized. One is the CS phase. This phase is induced by quantized vortices penetrating between the layers, and is characterized by $q \neq 0$ and $\delta \neq 0$. Although the CS phase can also be induced by the Rashba SOI through the paramagnetic effect [6], the orbital effect dominates the paramagnetic effect in the present system, i.e., the shift of q due to the orbital effect is much larger than that due to the paramagnetic effect. Consequently, in an intermediate magnetic field region of the trilayer system's phase diagram, the vortex-induced CS phase is stable. This phase is characterized by both magnitude and phase modulations of the order parameter, and is also referred to as the Josephson vortex phase. The other phase is the helical phase, which emerges in a higher magnetic field region of the phase diagram. As the quantized vortices penetrating between the layers effectively weaken the superconducting layer coupling (i.e., δ approaches zero with increasing $H^{\parallel}$), independent superconducting states are stabilized, instead of the CS phase with $\delta \neq 0$. Note that the superconductivity of the second layer (LO state) is already destroyed in the high magnetic-field region ($\mu_{\text{B}} H_{\text{c2}}^{\parallel} / k_{\text{B}} T_{\text{c0}} > 0.5$). This phase can be regarded as the helical phase, and is characterized by $q \neq 0$ and $\delta \approx 0$. Thus, with increasing $H^{\parallel}$ along the superconducting-normal phase boundary, the transition from the CS phase to the helical phase occurs following the transition from the BCS phase to the CS phase. The numerical calculations show that the upturn begins when δ becomes almost zero. Therefore, we conclude that the observed upturn corresponds to the transition from the CS phase to the helical phase, not to that from the BCS phase to the CS phase. We expect similar results for the bilayer system. Since the second layer does not play an important role on stabilizing the CS and helical phases, the trilayer system may be regarded as an effective bilayer system composed of the first and third layers.

In our trilayers, since the films are grown on GaAs substrates, the absolute values of the potential gradient in the z direction at the first and third layers may differ. This causes a difference between $|\alpha_1|$ and $|\alpha_3|$. We performed numerical calculations for $|\alpha_3| \neq |\alpha_1|$ (see Sec. IV of the Supplemental Material [22]). The sharp upturn occurs also for $(\alpha_1, \alpha_2, \alpha_3) = (125, 0, -100)$, $(125, 0, -75)$ and $(125, 0, +75)$ in meV (Fig. S1). We consider that the phase diagram obtained (Fig. S2) is essentially the same as that shown in Fig. 4(d), and that the breaking of the global inversion symmetry does not affect the conclusion.

In summary, we observed a sharp upturn in the measurements on the temperature dependence of $H_{\text{c2}}^{\parallel}$ for multiple monolayer films with layer-dependent Rashba SOIs. Using realistic numerical calculations with the BdG equations, we suggest that it corresponds to the transition from the complex-stripe phase to the helical phase. The numerical calculation including disorder effect is needed to make a quantitative comparison of the experimentally determined $H_{\text{c2}}^{\parallel}$ with the theoretical values. Our findings not only provide experimental evidence supporting the existence of the CS phase and the helical phase, but also offer a platform to study non-trivial superconductivity caused by symmetry breaking, including odd-parity pair-density-wave superconductivity [7] and 2D topological superconductivity [8,26,27] predicted for multilayer systems that are made up of the 2D Rashba superconductors.

[1] E. I. Rashba, Properties of semiconductors with an extremum loop. 1. cyclotron and combinational resonance in a magnetic field perpendicular to the plane of the loop, Sov. Phys. Solid State **2**, 1109 (1960).

[2] V. Barzykin and L. P. Gor'kov, Inhomogeneous Stripe Phase Revisited for Surface Superconductivity, Phys. Rev. Lett. **89**, 227002 (2002).

[3] O. V. Dimitrova and M. V. Feigel'man, Phase diagram of a surface superconductor in parallel magnetic field, JETP Lett. **78**, 637 (2003).

[4] Ol'ga Dimitrova and M. V. Feigel'man, Theory of a two-dimensional superconductor with broken inversion symmetry, Phys. Rev. B **76**, 014522 (2007).

[5] D. F. Agterberg and R. P. Kaur, Magnetic-field-induced helical and stripe phases in Rashba superconductors, Phys. Rev. B **75**, 064511 (2007).

[6] T. Yoshida, M. Sigrist, and Y. Yanase, Complex-stripe phases induced by staggered Rashba spin-orbit coupling, J. Phys. Soc. Jpn. **82**, 074714 (2013); see also JPSJ News Comments **10**, 09 (2013).

[7] T. Watanabe, T. Yoshida, and Y. Yanase, Odd-parity superconductivity by competing spin-orbit coupling and orbital effect in artificial heterostructures, Phys. Rev. B **92**, 174502 (2015).

[8] T. Yoshida, M. Sigrist, and Y. Yanase, Topological Crystalline Superconductivity in Locally Noncentrosymmetric Multilayer Superconductors, Phys. Rev. Lett. **115**, 027001 (2015).

[9] Y. Nakamura and Y. Yanase, Odd-parity superconductivity in bilayer transition metal dichalcogenides, Phys. Rev. B **96**, 054501 (2017).

[10] P. Fulde and R. A. Ferrell, Superconductivity in a strong spin-exchange field, Phys. Rev. **135**, A550 (1964).

[11] A. I. Larkin and Y. N. Ovchinnikov, Inhomogeneous state of superconductors, Zh. Eksp. Teor. Fiz. **47**, 1136 (1964) [Sov. Phys. JETP **20**, 762 (1965)].

[12] T. Zhang, P. Cheng, W.-J. Li, Y.-J. Sun, G. Wang, X.-G. Zhu, K. He, L. Wang, X. Ma, X. Chen, Y. Wang, Y. Liu, H.-Q. Lin, J.-F. Jia, and Q.-K. Xue, Superconductivity in one-atomic-layer metal films grown on Si(111), Nat. Phys. **6**, 104 (2010).

[13] T. Uchihashi, P. Mishra, M. Aono, and T. Nakayama, Macroscopic Superconducting Current Through a Silicon Surface Reconstruction with Indium Adatoms: Si(111)-($\sqrt{7} \times \sqrt{3}$)-In, Phys. Rev. Lett. **107**, 207001 (2011).

[14] M. Yamada, T. Hirahara, and S. Hasegawa, Magnetoresistance Measurements of a Superconducting Surface State of In-Induced and Pb-Induced Structures on Si(111), Phys. Rev. Lett. **110**, 237001 (2013).

[15] A. V. Matetskiy, S. Ichinokura, L. V. Bondarenko, A. Y. Tupchaya, D. V. Gruznev, A. V. Zotov, A. A. Saranin, R. Hobara, A. Takayama, and S. Hasegawa, Two-Dimensional Superconductor with a Giant Rashba Effect: One-Atom-Layer

Tl-Pb Compound on Si(111), Phys. Rev. Lett. **115**, 147003 (2015).

[16] T. Nakamura, H. Kim, S. Ichinokura, A. Takayama, A. V. Zotov, A. A. Saranin, Y. Hasegawa, and S. Hasegawa, Unconventional superconductivity at one-atomic-layer alloy Si(111)-$\sqrt{3} \times \sqrt{3}$-(Tl, Pb), Phys. Rev. B **98**, 134505 (2018).

[17] A. M. Clogston, Upper Limit for the Critical Field in Hard Superconductors, Phys. Rev. Lett. **9**, 266 (1962).

[18] B. S. Chandrasekhar, A note on the maximum critical field of high-field superconductors, Appl. Phys. Lett. **1**, 7 (1962).

[19] T. Sekihara, R. Masutomi, and T. Okamoto, Two-Dimensional Superconducting State of Monolayer Pb Films Grown on GaAs(110) in a Strong Parallel Magnetic Field, Phys. Rev. Lett. **111**, 057005 (2013).

[20] T. Sekihara, T. Miyake, R. Masutomi, and T. Okamoto, Effect of parallel magnetic field on superconductivity of ultrathin metal films grown on a cleaved GaAs surface, J. Phys. Soc. Jpn. **84**, 064710 (2015).

[21] R. Masutomi and T. Okamoto, Adsorbate-induced quantum Hall system probed by scanning tunneling spectroscopy combined with transport measurements, Appl. Phys. Lett. **106**, 251602 (2015).

[22] See Supplemental Material at http://link.aps.org/supplemental/10.1103/PhysRevB.101.184502 for angular alignment and the angular dependence of $H_{c2}(T)$, sample preparation and properties, model and formulation, and effects of global inversion symmetry breaking.

[23] M. Niwata, R. Masutomi, and T. Okamoto, Magnetic-Field-Induced Superconductivity in Ultrathin Pb Films with Magnetic Impurities, Phys. Rev. Lett. **119**, 257001 (2017); see also Supplemental Material at http://link.aps.org/supplemental/10.1103/PhysRevB.101.184502.

[24] The perpendicular field dependence of R_{sq} in bilayers and trilayers is similar to that observed in monolayers (e.g., Refs. [14,15,19]). It seems reasonable that the Josephson coupling does not have a significant effect on the vortex motion in a perpendicular magnetic field.

[25] K. Yaji, Y. Ohtsubo, S. Hatta, H. Okuyama, K. Miyamoto, T. Okuda, A. Kimura, H. Namatame, M. Taniguchi, and T. Aruga, Large Rashba spin splitting of a metallic surface-state band on a semiconductor surface, Nat. Commun. **1**, 17 (2010).

[26] S. Nakosai, Y. Tanaka, and N. Nagaosa, Topological Superconductivity in Bilayer Rashba System, Phys. Rev. Lett. **108**, 147003 (2012).

[27] T. Yoshida, A. Daido, Y. Yanase, and N. Kawakami, Fate of Majorana Modes in CeCoIn$_5$/YbCoIn$_5$ Superlattices: A Test Bed for the Reduction of Topological Classification, Phys. Rev. Lett. **118**, 147001 (2017).